Infrared imagery applied to a large buoyant plume

Brustet J.-M., B. Benech, P. Waldteufel

Infrared Imagery Applied to A Large Buoyant Plume

J.-M. BRUSTET

Département des Sciences de l'Atmosphère, Université Paul Sabatier, 31000 Toulouse, France

B. BENECH AND P. WALDTEUFEL

Observatoire du Puy de Dôme, Centre de Recherches Atmosphériques, 65300 Lannemezan, France

(Manuscript received 11 November 1980)

ABSTRACT

The possibility of applying infrared imagery to the study of a large, hot plume materialized by carbon particles resulting from the incomplete combustion of fuel oil is investigated.

In a specific case (the PROSERPINE experiment), due to the high carbon particle content, the lower part of the plume acts as a semi-opaque target. Using an infrared camera equipped with a detector sensitive in the 2–5.8 μm band, the thermal images are found to yield a plume geometry in good agreement with visible contours retrieved from visible photographs.

Thermal images provide access to the internal structure of a plume, down to scales which depend on the plume opacity. It appears that IR imagery is able to yield improved information concerning the turbulent fields of motion and temperature.

1. Introduction

Among the difficult problems to deal with in fluid mechanics, particularly in the case of the atmosphere, is the fairly typical three-dimensional development of a perturbation induced in the planetary boundary layer by a thermal discontinuity created near ground level. *In situ* measurements carried out by instrumented aircraft are of an instantaneous nature, and therefore are difficult to interpret. Whenever possible, they should be supplemented with more continuous, remote sensing techniques in order to provide a fuller coverage in time and space. For such techniques to be effective, however, the phenomenon under study should present specific characteristics allowing its detection.

In this paper, we investigate the possibility of applying infrared (IR) imagery to the study of the properties of a large, hot plume materialized by carbon particles (smoke) which result from the incomplete combustion of fuel oil. Basically, infrared remote sensing gives access to the thermal field of a target. When studying plumes, the knowledge of this field might be a valuable addition to that of the wind field, which can often be retrieved, for example, from the motion of optical tracers through photogrammetric techniques.

Thermal imagery is being used in many domains [e.g., remote sensing of the earth from space (Smith *et al.*, 1970), medical, scientific (Cagnasso *et al.*, 1976) and military applications]. Nearest to the present case is probably the study of cloud masses, using images collected by meteorological satellites (e.g., Liou, 1977).

2. Theory of the measurement

When attempting to estimate the physical temperature of a plume in the atmosphere through thermal imagery, one has to consider both the atmospheric transparency and the radiative nature of the target.

a. The radiative transfer equation

The energy flux dW received by a detector with area A from a blackbody target with temperature T, in the solid angle $d\Omega$ (Fig. 1), in a spectral interval $d\lambda$, can be written

$$dW = I(T, \lambda)Ad\Omega d\lambda, \tag{1}$$

where $I(T, \lambda)$ is the Planck radiance function.

Here we shall be concerned with a spectral interval in the near infrared which includes strong absorption bands. We define the transmission coefficient τ for a length s along the optical path

$$\tau = \exp\left[-\int_0^s \rho(s')k(\lambda, s')ds'\right], \tag{2}$$

where $\rho(s)$ and $k(\lambda, s)$ are the density and spectral attenuation coefficient of the absorbing gas. While the corresponding emission coefficient $\epsilon(\epsilon = 1 - \tau)$

0021-8952/81/050571-10$06.50

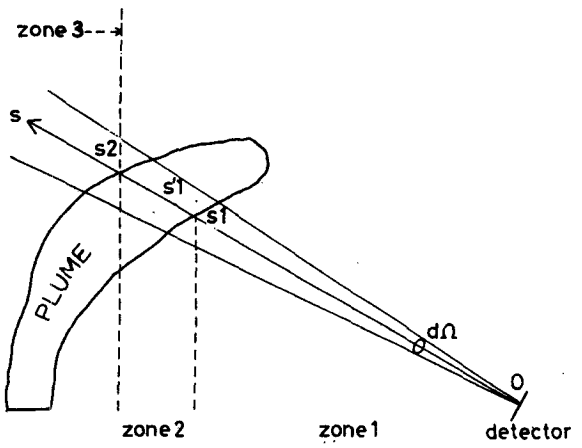

FIG. 1. The energy flux received by a detector (A) in the solid angle $d\Omega$ comes from three zones encountered sequentially along the optical path.

depends on the medium properties, it does not depend explicitly on its temperature.

In the plume case, the total received flux is proportional to the sum of contributions coming from three zones encountered sequentially along the optical path (Fig. 1): zone 1 is located between the receiver and the plume (segment Os_1), zone 2 is the plume thickness (segment s_1s_2) and zone 3 corresponds to the atmosphere behind the plume.

We assume zones 1 and 2 are isothermal with temperatures T_a and T_p, and define their emissivities $\epsilon_a(\lambda, Os_1)$ and $\epsilon_p(\lambda, s_1s_2)$. Then the total energy flux Φ_T reaching the detector consists of three parts:

$$dW/(Ad\Omega d\lambda) = \Phi_T = \Phi_1 + \Phi_2 + \Phi_3, \quad (3)$$

with

$$\left.\begin{aligned}\Phi_1 &= I(T_a, \lambda)\epsilon_a(\lambda, Os_1)\\ \Phi_2 &= I(T_p, \lambda)\epsilon_p(\lambda, s_1s_2)[1 - \epsilon_a(\lambda, Os_1)]\\ \Phi_3 &= \phi_4 \times [1 - \epsilon_p(\lambda, s_1s_2)] \times [1 - \epsilon_a(\lambda, Os_1)]\end{aligned}\right\} \quad (4)$$

The flux ϕ_4 incident on the plume results from contributions over the whole atmospheric depth, including clouds and scattered sun radiation; it need not be detailed here.

Possible sources for scattered radiation along the Os_2 part of the path may originate either from the sun or from the flames in the combustion zone. In the latter case, rough calculations show the scattered flux to be two orders of magnitude below the flux thermally radiated by the plume, with the exception of a few tens of meters just above the combustion zone. In the case of the sun, the small fraction of incident radiation present (for $\lambda > 2.0\ \mu$m) at ground level (estimated for relevant elevations) might induce scattering contributions one order of magnitude below the thermal plume radiation. In the examples presented below, however, photogrametric recordings show the sky to be completely overcast.

Eq. (3) has further to be integrated over spectral interval and solid angle. Before accounting for these and formulating hypotheses concerning the actual infrared characteristics of the plume, it is worth considering possible simplifications, depending on the transparency assumed for the plume.

b. Discussion

If the plume is assumed to be a plane blackbody perpendicular to the line of sight, its emission coefficient is equal to unity and the third contribution vanishes:

$$\Phi = \Phi_1 + \Phi_2 = I(T_a, \lambda)\epsilon_a(\lambda, s_1) + I(T_p, \lambda)[1 - \epsilon_a(\lambda, s_1)]. \quad (5)$$

The atmospheric emissivity ϵ_a can be inferred from both specific physical parameters supplied by nearby radiosonde measurements and average, climatologic information (e.g., CO_2 or water vapor content). We shall use model results of Wyatt *et al.* (1964) and Selby and McClatchey (1972)[1] under the conditions closest to our experiment. $I(T_a, \lambda)$ is computed using the $T(z)$ measurements; in our case the relevant atmospheric layer does not extend above a 400 m altitude and we shall use the mean temperature within this layer.

The plumes under consideration consisted of expanding smoke containing carbon particles and an excess of carbon dioxide and water vapor. Clearly, assuming such a target to be a perfect plane blackbody at every height represents an oversimplification.

The plume depth s_1s_1' responsible for the emitted radiation is finite. It increases as the concentration of particles and gas in the plume decreases. Whenever the target is opaque ($s_1s_1' < s_1s_2$), ϵ_p is equal to unity and the plume temperature can be estimated in the same manner as above.

In the general case, the plume is to be considered as a transparent, greybody and Eq. (3) should be used without any simplification. In addition to the previous case, one then has to determine ϵ_p for the plume depth s_1s_2. This can be done fairly simply, provided the plume emissivity can be parameterized as a function of the concentration of specific plume components. However, possible inhomogeneities in the background radiation ϕ_4 are likely to make the interpretation difficult.

3. The experiment

The previous considerations were applied to the PROSERPINE experiment, which was carried out on the CESTA (Landes, southwestern France) ex-

[1] Selby, J. E. A., and R. A. MacClatchey, 1972: Atmospheric transmittance from 0.25 to 28.5 μm; computer code LOWTRAN 2. A. F. Cambridge Research Laboratories, AFCRL Rep. 72-0745, 77 pp.

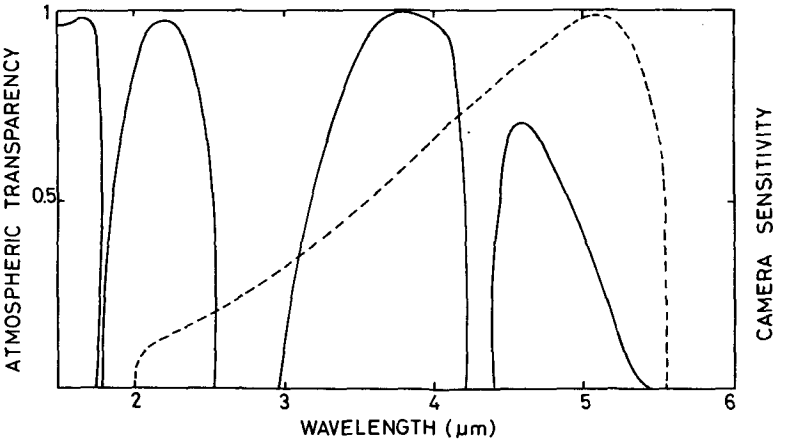

FIG. 2. Left scale (continuous line): Calculated atmospheric transparency for an horizontal path and precipitable water content (0.23×10^{-2} mm m^{-1}, length 2.8 km). Right scale (dotted line): Relative sensitivity function of the camera.

perimental site in February 1977.[2] The heat source consisted of a fuel oil layer, stretched over the surface of a 1920 m^2 water tank. The fuel was ignited in six locations simultaneously and the mean observation time lasted 15 min after the ignition was completed. Five tests were made with these conditions.

a. Experimental environment

- Atmosphere characteristics: Surface conditions were characterized by continuous records of the wind speed and direction, hygrometry, temperature and pressure. Measurements aloft consisted of radiosonde launchings and *in situ* observations carried out by an instrumented aircraft.
- Heat source: Direct temperature measurements were made above the fuel oil layer using a Chromel-Alumel thermocouple, at a 1–2 m height over various points of the tank, and up to 10 m using a mast located in its center. The flame temperature could be remotely monitored using pyrometric devices.
- Plume: The plume geometry was determined using two photogrammetric stations aimed perpendicularly to the prevailing wind direction. The main parameters estimated are the culminating altitude, the plume radius as a function of height and the vertical velocity.

In situ measurements were carried out by the instrumented CESSNA 206 airplane of the French Météorologie Nationale. This included information on the variation of thermodynamical parameters over horizontal intersections of the plume. The aircraft was further equipped with an aerosol sampling device; the samples were collected on filters, later treated (metalized) and inspected with a scanning electron microscope.

b. Infrared imagery

On the CESTA site, we used an AGA infrared movie camera equipped with an indium-antimony (Sb-In) detector sensitive in the 2–5.8 μm band, which includes both absorbing and transparent spectral regions (Fig. 2). The germanium objective has a 25° aperture; this corresponds, for a 900 m distance to the source, to an approximate 400 m × 400 m field of view.

Several diaphragms ($f/1.8$ to $f/18$) are available allowing use of the camera for various temperatures ranges. The selected diaphragm ($f/18$) corresponds to temperatures within the [−30°C, +190°C] interval.

The sensitivity of an infrared camera is determined by 1) a geometrical factor which depends on the aperture and the surface of the sensitive area; and 2) the spectral sensitivity of the detector and optics.

Both factors must be considered when calibrating the camera. Fig. 3 shows the received signal in relative thermal units as a function of temperature. The minimum detectable temperature difference is 0.2°C, around a 30°C value. The calibration is made by pointing at a reference blackbody with known temperature before each observation.

Video signal and synchronization marks generated by the camera are recorded on analog tape with a 16 images s^{-1} acquisition rate. Each image contains 80 lines of video information. These data were digitized and processed, leading to the construction of digital images. Eighty data points were sampled for each line; thus each pixel content represents the energy flux received from a solid angle with a 5.5 mrad size.

The digital images or thermograms provide our basic support for the analysis of infrared data.

[2] B. Benech, J. M. Brustet and Pham Van Dinh, 1977: Operation PROSERPINE. Ministère de l'Intérieur (Direction de la Sécurité Civile), Paris, 73–98.

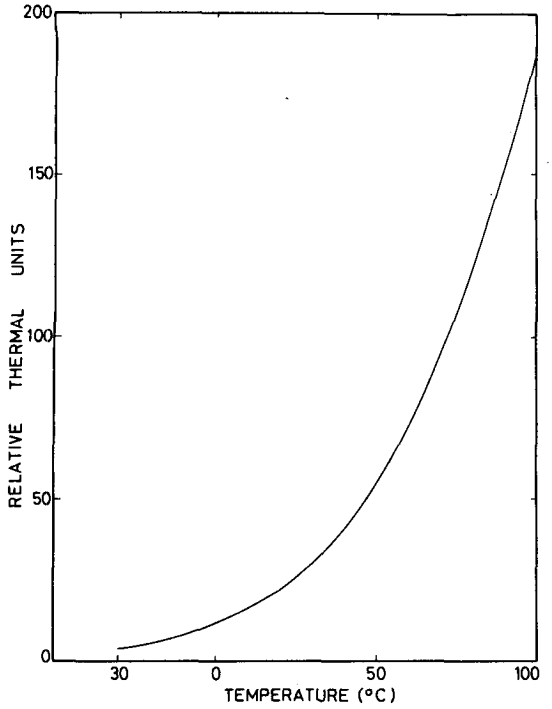

FIG. 3. Calibration curve of the IR camera.

c. Processing hypotheses

In order to interpret quantitatively the thermograms, we need to specify further the radiative properties of both the plume and the atmosphere.

Concerning the plume, the main question is to determine whether it can be considered as a semidense source. Both the gases and aerosol resulting from the combustion contribute to the plume opacity.

Accounting for the heat source area, the combustion rate (2.4 metric tons per minute), the chemical nature of the fuel (assimilated to $C_{16}H_{32}$) and the source efficiency (the air/fuel Bonnier richness is 0.5 for a flame temperature of 12 000°C[3]), the CO_2 and H_2O fluxes liberated in the plume are of the order of 160 $m^3\ s^{-1}$. Since the total plume flow at a 200 m altitude is $\sim 8 \times 10^4\ m^3\ s^{-1}$ (from evaluated 140 m diameter and 5 m s^{-1} ascending velocity), the resulting CO_2 relative concentration is 2×10^{-3}, i.e., seven times more than in the undisturbed atmosphere; the excess water vapor content is 0.65 g m^{-3} (cf. 6 g m^{-3} in the undisturbed atmosphere at that time).

We have estimated the penetration depth due to excess gases for a spectral interval matched to the characteristics of our camera (4.5–5 μm), using data provided by Passman and Larmore (1956), and found it to be always much larger than the plume diameter D.

[3] Van Dinh, Pham, and B. Benech, 1978: Étude de la combustion du fuel-oil domestique à l'air libre. Note I.O.P.G., No. 48, Institut et Observatoire du Puy de Dôme, Clermont-Ferrand, 60 p.

The size histogram of some samples of carbon particles taken on 23 February 1977 at a 300 m height in the rising plume near its axis is shown in Fig. 4. The size spectrum is centered between 0.5 and 1 μm, and spreads between 0.25 and 16 μm. Whereas the size distribution is representative of the actual situation within the plume, the number density is substantially underestimated (due to the difficulty of matching accurately the sampling period and the time that the plane flew inside the plume). Samples taken at various heights up to 600 m yielded size distributions similar to the one shown in Fig. 4.

From these data, we derive a crude estimate of the optical depth due to smoke particles by neglecting scattering and masking effects (this tends to underestimate the result) and assuming that the particle concentration is homogeneous throughout the plume. We then sum every particle cross section along a column with surface unit basis, and compute the depth D_s which would result in a total cross section equal to unity.

The results are shown on Table 1 for various heights, together with plume diameter values D estimated by photogrammetry. It can be seen that, up to 500 m, D_s is always less than half the plume diameter. Thus, in this altitude range, part of the plume can be treated as a blackbody ($\epsilon_p = 1$).

When pointing at the plume, the energy flux received by the detector corresponds to an apparent temperature T_p' intermediate between T_a and the actual plume temperature T_p. This is illustrated by

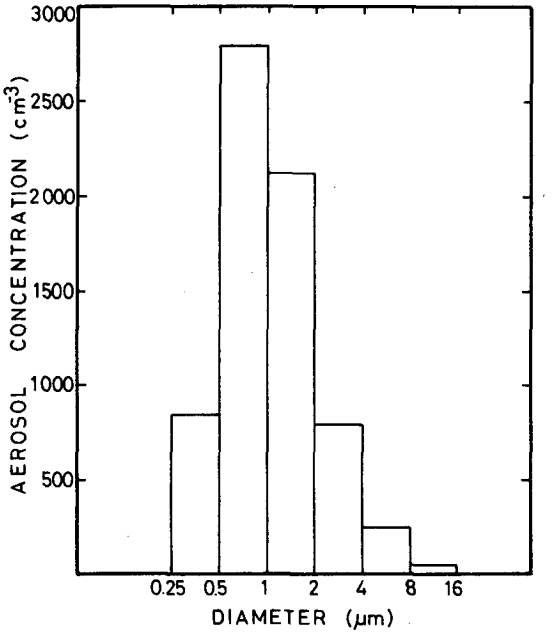

FIG. 4. Smoke particles concentration versus particle diameter: samples taken on 23 February 1977 at a 300 m height in the rising plume during the PROSERPINE experiment.

TABLE 1. Observed plume diameter for various altitudes, compared to the required plume penetration for opacity due to smoke particles.

Altitude (m)	Observed plume diameter D (m)	Plume penetration D_s (m)
0	40	
300	180	30
500	320	150
600	440	270

Fig. 5 which shows, as a function of T_p, the received energy flux computed by integrating Eq. (3) over λ, accounting for the camera sensitivity function, in absence (curve a) and in presence (curve b) of the atmosphere. The two curves intersect when $T_a = T_p$; for $T_p > T_a$ the apparent temperature is less than T_p, and conversely. This diagram can be used for the retrieval of T_p.

In our experimental conditions (target-camera distance of the order of 1 km), the absorption by atmospheric gases is ~50%; additional absorption by atmospheric aerosol has been found of the order of 3% (using data from Junge, 1963) and eventually was neglected.

When looking outside the plume, the received energy results from emission by the cloud deck, as well as absorption and emission throughout the underlying atmospheric layer. From the variation of the received energy with elevation angle, it is possible, in principle, to retrieve some information about the temperature profile by considering emission/absorption processes of the carbon dioxide in a stratified atmosphere hypothesis (Deschamps and Brogniez, 1972). The spectral interval of our camera, however, is inadequate for addressing this problem.

4. Results

a. General structure of a thermogram

A thermogram (Fig. 6) is a matrix of numerical figures which are proportional to the energy received by the detector in each pixel. Isocontours for this energy are lines of equal apparent temperature and will be referred to as isotherms in the following.

The general shape of the plume is seen clearly on Fig. 6 as an elongated, tilted zone delineated by the isotherms. This shape is in excellent qualitative agreement with the optical contour of the plume, as shown in Fig. 7 by a visible photograph taken from a location near the camera at about the same time.

In the region outside the plume, where the received energy involves radiative transfer throughout the troposphere, the apparent temperature decreases smoothly as the elevation angle increases. When

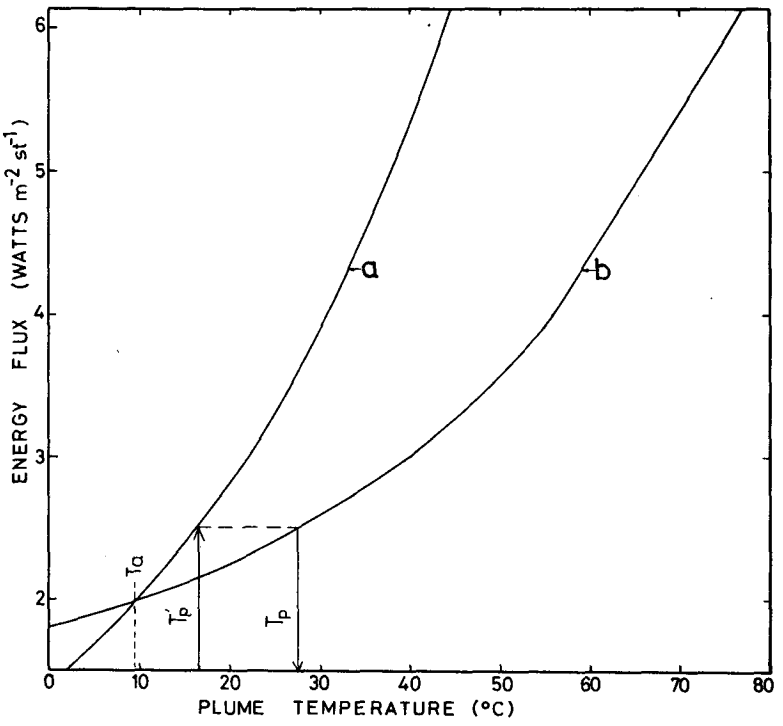

FIG. 5. Energy flux computed from Eq. (3), accounting for the camera sensitivity function. Curve a: in the absence of an atmosphere (i.e., Planck function × camera function); curve b: in the presence of an atmosphere (mean temperature 10°C, humidity 65%, path length: 1000 m).

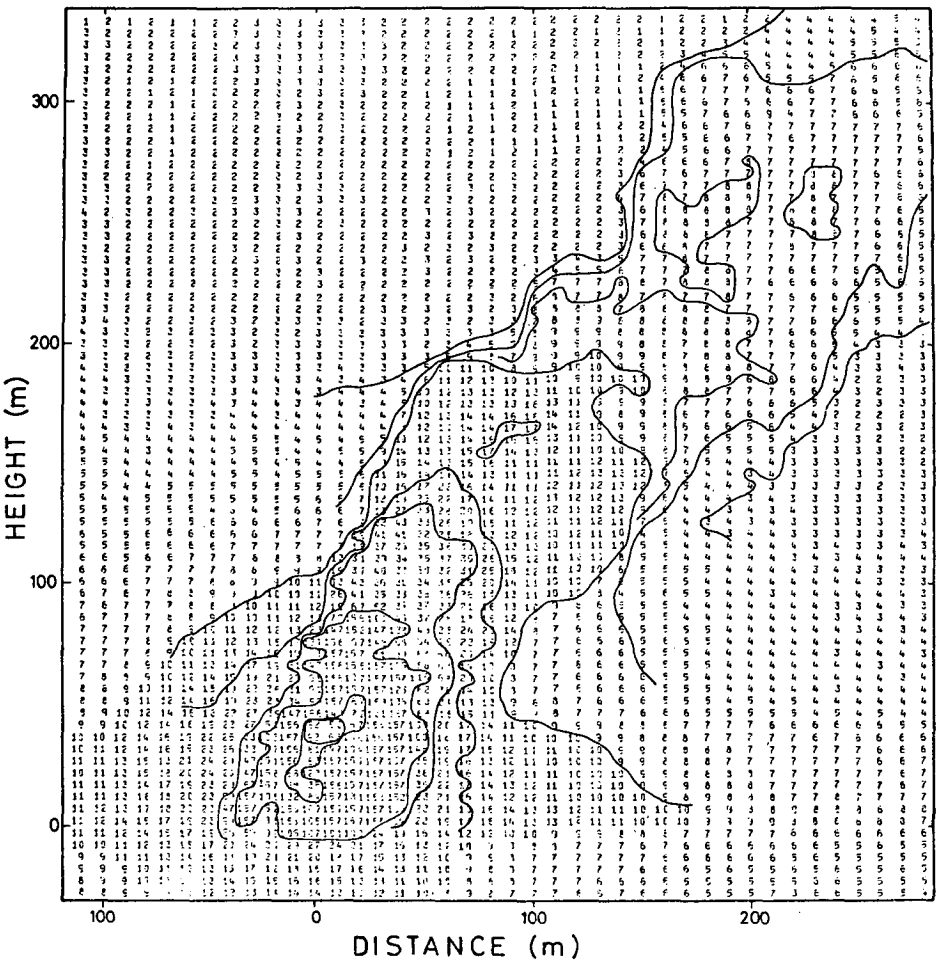

FIG. 6. A thermogram retrieved from IR data. Each numerical value is proportional to the energy received by the detector from a 5.5 mrad solid angle. Isocontours for this energy are lines of equal apparent temperature (isotherms); they are drawn in the plume boundary zone (semi-transparent region) and in the internal plume region (semi-dense region). The zone surrounding the heat source is too hot for our sensitivity range.

approaching the plume, we observe in the boundary zone a steep temperature gradient. In this zone the plume is a semi-transparent target, and the apparent temperature is not easy to interpret.

We now concentrate on the internal region, where the plume can be treated as an opaque target and the significance of apparent temperature has been discussed above. Since the zone surrounding the heat source is too hot for our sensitivity range and the upper part of the plume ceases to be opaque, we shall restrict ourselves for the time being to the altitude range between 100 and 300 m. In this range, we now investigate the main features of variations in time and space of the apparent temperature field.

b. *Temperature gradients*

The resolution cell seen by the camera corresponds to a volume with approximate size 5 m × 5 m × D_s (the depth D_s is defined in Table 1). The true temperature T_p, when retrieved from T_p', will be an average temperature within this volume.

Table 2 presents a synoptic summary of temperature values obtained for various altitudes using every available measurement. These include a T_a profile outside the plume (radiosonde), a few T_p values measured by the aircraft when crossing the plume (the maximum recorded value was selected), thermocouple and radiometric data near the heat source up to 15 m, and infrared imagery results. The latter were obtained from two images taken at 1 min interval, and the true temperature was retrieved from T_p' for various levels up to 250 m. Two values are indicated; one is taken along the plume axis (i.e., center of apparent diameter) and the other is the maximum value recorded at each level.

Toward the plume bottom infrared data show a slower decrease with altitude (70°C m^{-1}) than do the

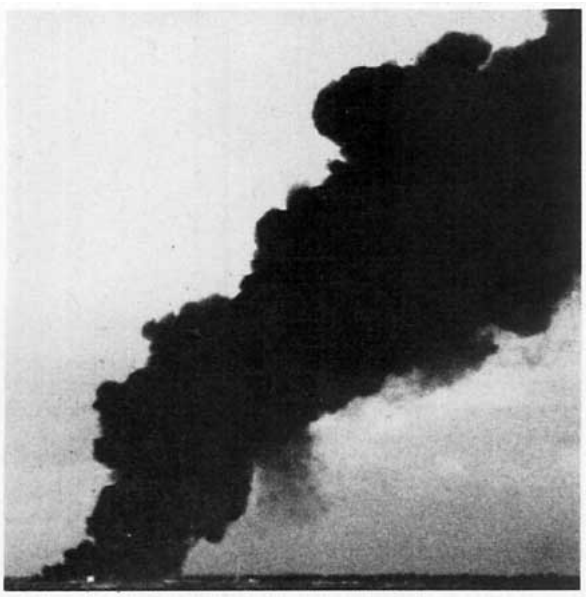

FIG. 7. A photograph of the plume on 23 February 1977 taken from a photogrammetric station near the IR camera, within a few minutes of the thermogram shown in Fig. 6.

thermocouple measurements (100°C m^{-1}). Nevertheless, the absolute magnitude in the common altitude range is in fair agreement.

Only infrared imagery data are available in the zone extending from 15 m up to the 245 m level, where the airplane supplied a single measurement. The T_p values along the axis are consistent with a smooth overall temperature profile within the plume, and the agreement with the plane measurement is fair. On the other hand, the maximum temperature recorded at each level may be substantially higher and more erratic. The variability within a horizontal plume section is further illustrated by Fig. 8, which shows every measurement obtained over a 1 min period (using a sample of 60 thermograms) for several levels. The median of values measured along the plume axis exhibits a good continuity with altitude, as well as the median of highest values recorded at each level. There is a broad scattering of the data points, especially at lower levels; the trend for the temperature distribution is to become narrower as the altitude increases.

Three temperature cross sections taken at 2 s intervals at the 250 m level are shown in Fig. 9. These curves illustrate first the transition on each side of the plume from the internal (opaque) zone, which concerns our assumptions about the $T_p' \rightarrow T_p$ relationship, to the plume-free zone across the semi-dense boundary region. We consider the region to be opaque where D_s is smaller than $s_1 s_2$, estimated from photogrammetry.

Also apparent in Fig. 9 are horizontal tempera-

TABLE 2. Temperature data obtained on 23 February 1977 concerning the atmosphere (radiosondes, aircraft soundings), the heat source vicinity (thermocouples, radiometers), and the plume (aircraft, IR imagery; two thermograms were taken 1 min apart).

	Temperature (°C)							
			Plume					
					IR imagery			
	Atmosphere				Thermogram 1		Thermogram 2	
Altitude (m)	Radiosondes	Aircraft	Thermocouples	Pyrometers	Axis	Maximum	Axis	Maximum
0	10		1250	1300*				
1			1250					
2			1050					
5			1100					
7.5			280					
10			160					
15				600**				
80	8.8							
100					38	46	54	54
120					36	41	34	34
150					25	35	34	40
190	8.1							
200					22	24	16	19
240	7.8	10.5			14	14	12	16
300	7.4	9.8						
450	6.1							
520	4.9	6.1						
590	4.4	4.9						

* THERMODOT TD9 pyrometer.
** IRCON 700 AC pyrometer.

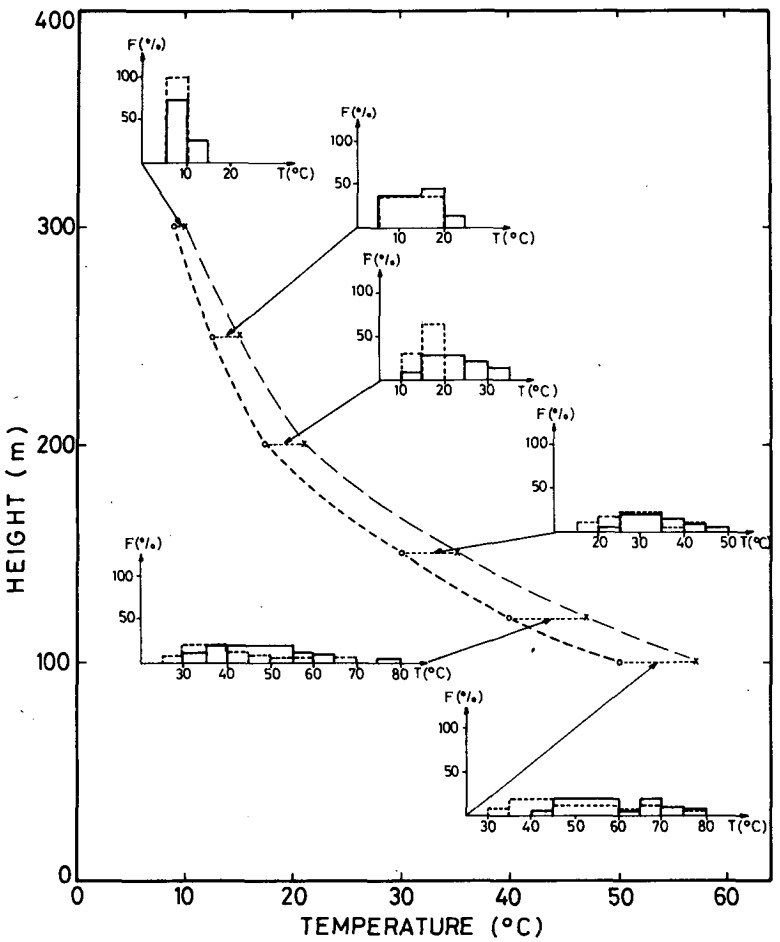

FIG. 8. IR temperature data at selected levels in the plume, from 60 thermograms. At each level are shown histograms of the axis value (continuous) and the highest value across the plume (dotted). The altitude variation of the median of both distributions is indicated by circles and crosses, respectively.

ture gradients inside the plume. Warmer zones are located upwind with respect to the ambient air circulation: the scale of irregularities is roughly half the apparent plume diameter. Actual heterogeneities inside the plume are likely to be more marked than appears on the infrared images, due to smoothing effects introduced by volume integration and numerical interpolation.

c. *Warm bubbles propagating up the plume*

In many cases, warmer zones of limited extent can be isolated by closed isotherms inside the infrared plume structure. Although the exact size of such features is difficult to define since their boundaries blend in smoothly with the surroundings, their identification is clearly demonstrated by the possibility of unambiguously tracking their evolution and motion with time, on successive thermograms, over periods of several tens of seconds.

Assuming that the location and apparent temperature of the hottest pixel within such a warm bubble (or cell) is representative of its evolution, it is possible to characterize crudely dynamic and thermal variations. From a sample of images covering a 2 min period, we were able to identify and track 20 cells in the 100–300 m altitude range. The cell trajectories, although lacking perfect regularity, can always be likened without large distortion to average, linear motions. Several warm cells (most often two, sometimes up to three or even four) can be present in the plume at the same time. Coexisting cells may have different ascending velocities. This is illustrated in Fig. 10 by the histogram of observed velocities. The existence of two modes (4–5 m s^{-1} and 7–8 m s^{-1}) is suggested.

It would be desirable to characterize the warm bubbles and their displacement in a more objective manner. To this purpose, we have cross-correlated thermal fluctuation time series measured at three

pairs of locations; in each case, the altitudes are 100 and 300 m, and the two locations are along a line parallel to the plume axis. A significant peak in the cross-correlation functions is indeed found, with a mode (see Fig. 10) centered on 7–9 m s^{-1}. This certainly is compatible with the result of empirical tracking of warm bubbles; therefore, the cross-correlation method seems a promising tool for systematic investigation of thermal patterns propagating inside the plume.

5. Discussion and conclusion

In this paper, we have first discussed briefly the radiative transfer aspects of thermal plume imagery and shown that in a specific experimental case, it was possible to consider a given region of the plume as a semi-opaque target due to the high content of carbon particles. Results of a preliminary interpretation of thermal imagery are twofold:

- The thermal image is correct in a semi-quantitative way. This is illustrated by the good agreement between thermograms and visible photographs showing the plume contours (Fig. 6 and 7), and by the continuity between IR values and independent temperature measurements (Table 2, Fig. 8).
- A thermal image provides access to the internal structure of a plume, down to scales which are substantially smaller than the plume size; the lower limit depends on the plume opacity. In these conditions, large fluctuations of the temperature are brought to evidence, as well as the fact that such fluctuations may propagate into the plume during a sizable time, with quite variable velocities.

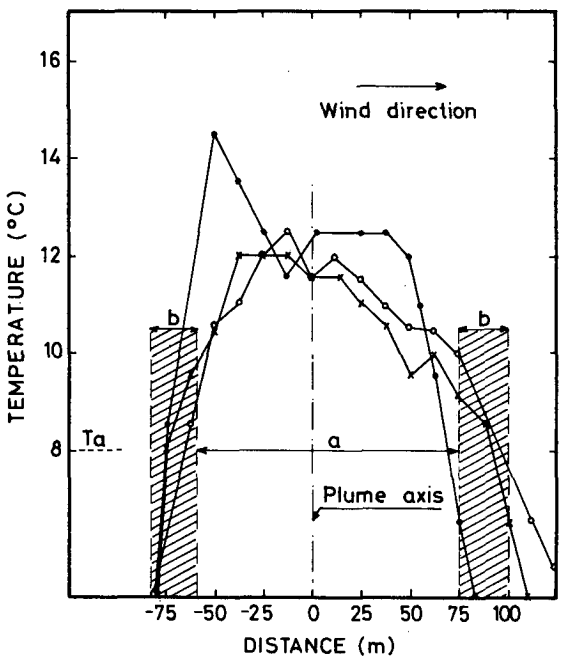

FIG. 9. Three temperature cross sections taken at 2 s intervals at the 250 m level on 23 February 1977 in the plume, across the internal (a) and transition (b) zones.

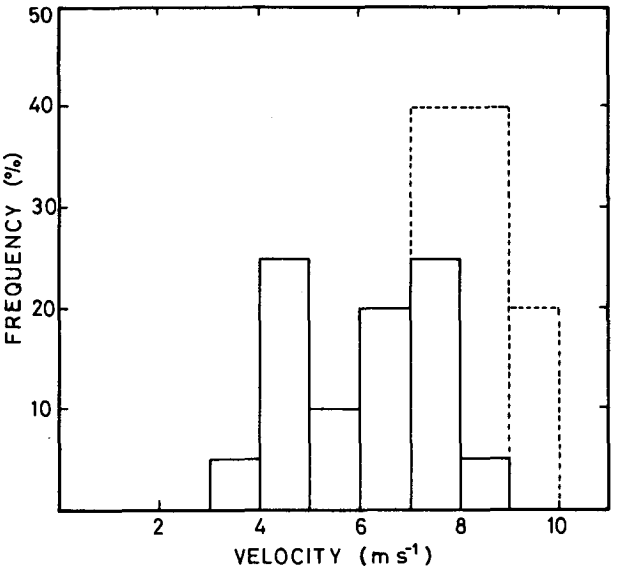

FIG. 10. Frequency distributions of vertical velocities inside the plume in the 200–300 m height range: motions of warm bubbles detected visually (solid line) and derived from cross correlation analysis (dashed line).

It appears therefore that IR imagery yields improved information concerning the structure of the turbulent fields of motion and temperature. Moreover, the amplitude of observed fluctuations suggests that whenever possible they should be considered to some extent when attempting to establish even a bulk energy budget for the plume.

Most of the data provided by IR imagery are unique. However, part of the observed results, especially concerning the motion field, can be compared with independent data (e.g., photogrammetry, chaff tracking). Such comparisons will be carried out in the future.

Finally, we are aware that it is difficult to obtain, in the case presented here, reliable, quantitative temperature values. This is mainly due to the attenuation which occurs within the lower atmosphere, as well as the contribution of scattered sun radiation, for the 2–6 μm spectral interval.

The influence of both factors is greatly decreased in the 8–12 μm band. For example, with our experimental conditions, the mean atmospheric transparency would be 85% in such a case, versus 45% for the 4.4–5.3 μm band (after Wyatt *et al.*, 1964).

Future experiments will be carried out using a 10 μm camera. We expect that in this way the quantitatve significance of IR data will be improved; this will be valuable when comparing the observed temperature field with results predicted by plume numerical models.

Acknowledgments. This work has been supported by Electricité de France, Département des Echanges Atmosphériques et Aquatiques.

We wish to express our thanks to members from the Institut et Observatoire de Physique du Globe du Puy de Dôme and from Département des Sciences de l'Atmosphère de l'Université Paul Sabatier (Toulouse) who took part in this project.

REFERENCES

Cagnasso, A., G. Canevet, Y. Jullien and P. Amalric, 1976: Application de la thermovision à la mécanique vibratoire. *Rev. Acoust.*, **39**, 269–271.

Deschamps, P. Y., and G. Brogniez, 1972: Détermination du profil vertical de température de l'atmosphère à partir du sol d'après l'émission infrarouge du CO_2. Méthode d'inversion de l'équation de transfert du rayonnement. *J. Rech. Atmos.*, Nos. 1–3, 117–132.

Junge, C. E., 1963: *Air Chemistry and Radioactivity*. Academic Press, p. 117.

Kuo-Nan Liou, 1977: Remote sensing of the thickness and composition of cirrus clouds from satellites. *J. Appl. Meteor.*, **16**, 91–99.

Passman, S., and L. Larmore, 1956: Atmospheric transmission. Rand Paper P. 897, Rand Corporation, Santa Monica, 11 July 1956 [Adapted by R. D. Hudson (1968); *Infrared System Engineering*. Wiley-Interscience, New York, 144–155.]

Smith, W. L., P. K. Rao, P. Koffler and W. R. Curtis, 1970: The determination of sea-surface temperature from satellite high resolution infrared window radiation measurements. *Mon. Wea. Rev.*, **98**, 604–611.

Wyatt, P. J., V. R. Stull and G. N. Plass, 1964: The infrared transmittance of water vapor. *Appl. Opt.*, **2**, 229–254.